PHYSICAL REVIEW B VOLUME 41, NUMBER 1 1 JANUARY 1990

Surface melting of Ni(110)

E. T. Chen, R. N. Barnett, and Uzi Landman
School of Physics, Georgia Institute of Technology, Atlanta, Georgia 30332
(Received 27 July 1989)

Disordering and melting of the surface of Ni(110) are investigated using molecular-dynamics simulations, in which the embedded-atom theory is used to describe the energetics and interatomic interactions. The surface region disorders at temperatures as low as 1450 K via the generation of vacancies accompanied by the formation of an adlayer. The development of a quasiliquid region exhibiting liquidlike energetic, structural, and transport properties, and whose thickness increases as the temperature approaches the melting point, is observed. It is concluded that the premelting of the surface occurs at $T \gtrsim 1700$ K.

I. INTRODUCTION

Although the melting of solids is one of the most common observations of a phase transition, the mechanism of melting is still an outstanding problem in condensed-matter physics.[1,2] While the suggestion that melting nucleates at the surface of the solid and then propagates inward and the idea that the surface of a solid may become liquid at a temperature below the (nominal) bulk melting point T_m dates back over a century,[3] a comprehensive understanding of the phenomena, at the microscopic level, is still lacking.

Surface melting, which can be viewed as the wetting of the solid-gas interface by the liquid (or quasiliquid, see the following) upon approaching the triple point, provides the opportunity for investigating surface phase transformations and solid-liquid interfaces using modern surface-science techniques. While numerous attempts to detect surface-initiated melting phenomena have been made,[4-6] it is only recently that direct observations of surface melting have been made on a microscopic level, employing atomically clean, well-characterized surfaces. The first direct observations[7-9] were made using Rutherford backscattering, in conjunction with shadowing and blocking. Since then, other techniques have been employed such as calorimetry,[10-15] ellipsometry,[16,17] electron diffraction,[18-22] microscopy,[23] neutron[24] and x-ray diffraction,[25,26] quasielastic neutron[27] and helium scattering,[27-29] and even visual inspection with the naked eye.[30,31]

The genesis of theoretical investigations of surface-melting phenomena may be traced to the classic paper by Burton, Cabrera, and Frank,[32] who pointed out that above a characteristic temperature, T_R, the structure of the surface region of a crystalline solid may depart from the structure corresponding to the terrace-ledge-kink (TLK) model due to a phase transition that they have termed as *surface melting*, and that has been later called the *roughening transition* (perhaps this is the cause of some confusion in the literature between the two terms,[1,2,6] which occasionally were taken to be synonymous). Surface melting, as distinguished from roughening, involves a lack of registry of the atoms in the premelted surface region with respect to the underlying crystal, resulting in liquidlike properties of that surface region. However, the atoms in the premelted finite-thickness film are influenced by the presence of the underlying crystal. Therefore the surface-melt layer at the initial stages of the process, should be regarded as a quasiliquid exhibiting structural, dynamical, and transport properties that are intermediate between those of the solid and the bulk liquid. It is the formation of the thin quasiliquid layer (QLL), whose thickness grows as the temperature approaches T_m, which one terms appropriately as surface premelting.[1]

While the Lindemann melting criterion,[33] applied to the surface region, has been used to rationalize the existence of surface premelting (due to the softening of vibrational modes near the surface, i.e., larger root-mean-square thermal displacements of surface atoms), the applicability of this criterion to surface melting shares the same deficiencies encountered in applying it to bulk solids.

Most theoretical approaches to surface melting are of thermodynamical[1,2,34-37] and/or phenomenological nature, including lattice dynamics and stability analysis,[38-40] lattice-gas models (employing the mean-field[41] and the cluster variation methods[42]), and Landau theory.[43-45] Microscopic descriptions of surface disordering and melting phenomena emerged from computer molecular-dynamics (MD) simulations, which until very recently[46] employed[47-51] simple pairwise interatomic interactions in the form of Lennard-Jones potentials, which are appropriate for the description of rare-gas solids and liquids, but are known to be inadequate for metals. It has also been emphasized[49] that faithful simulations of such phenomena require extra precautions in order to avoid erroneous conclusions originating from failure to achieve true equilibrium (i.e., insufficient simulation time span) and finite-size effects (i.e., cutoff of low-frequency, long-wavelength modes in the vibrational spectrum due to the finite size of the calculational cell and the application of periodic boundary conditions, and inherent fluctuations in system properties due to the finite number of particles

in the calculational cell).

In this study, we investigate, using MD simulations, the structural and dynamic behavior of the Ni(110) surface as the temperature of the system approaches the bulk melting point. In these investigations the energetics of the material is represented by the many-body potentials obtained via the embedded-atom method[52] (EAM), which has recently been applied with significant success in studies of various transition-metal systems, and in particular the equilibrium properties of solid-to-melt interfaces of nickel.[53] Following a brief description in Sec. II of the EAM and the MD simulation method, we present in Sec. III results indicating surface premelting close to, but below, the bulk melting point, as reflected in structural and atomic transport properties, and the formation of a quasiliquid region. Our results are summarized in Sec. IV.

II. METHOD

The embedded-atom method[52] (EAM) is a semiempirical method that provides a convenient framework for atomistic calculations of metallic systems. In this method the dominant contribution to the energy of the metal is viewed as the energy to embed an atom into the local electron density provided by the other atoms of the system, represented by an embedding energy function F, which is supplemented by short-range, two-body interactions due to core-core repulsion, Φ. The basic idea underlying this method is thus the same as that which motivated the development of the earlier effective medium theory (EMT),[54] and both find their roots in the density functional theory.[55]

The cohesive energy $E_{\rm coh}$ of the metal is given in EAM by the ansatz

$$E_{\rm coh}=\sum_i \left[F_i \left[\sum_{j\neq i} \rho_j^a(R_{ij}) \right] + \tfrac{1}{2} \sum_{j(i\neq j)} \phi_{ij}(R_{ij}) \right] , \quad (1)$$

where ρ^a is the spherically averaged atomic electron density, and R_{ij} is the distance between atoms i and j, located at $\mathbf{R}_i$ and $\mathbf{R}_j$. Thus the background density for each atom i is determined as the superposition of atomic density tails from the other atoms, evaluated at the nucleus of the ith atom. In the EAM the functions F and ϕ are determined by choosing for them functional forms that meet certain general requirements and fitting parameters in these functions to a number of bulk equilibrium properties of the solid such as lattice constant, heat of sublimation, elastic constants, vacancy-formation energy, etc. From the several parametrization procedures that have been discussed,[52] we have chosen the one described by Foiles[56] in this study of liquid transition metals. These potentials were used by us recently[53] in studies of the structure and energetics of the equilibrium crystal to melt interfaces of Ni(001) and Ni(111), and the melt-to-vapor interface of nickel. Furthermore, from molecular-dynamics simulations of nickel, employing the aforementioned parametrized[56] EAM potentials, we have determined that the melting temperature of the bulk metal is 1733±22 K, and the latent heating of melting is 0.19 eV/atom is in good agreement with the experimental values[57] ($T_m=1725$ K and $\Delta H_m=0.182$ eV/atom).

The total energy expression given in Eq. (1), with the above-mentioned parametrization, is then employed in a molecular-dynamics simulation in which the temporal evolution of the system is followed via integration of the classical equations of motion for the atoms. In our molecular-dynamics simulations the semi-infinite system is modeled via a thick slab (15 layers with 70 atoms per layer) of interacting dynamic particles, exposing the (110) surface, which in addition interact with five crystalline layers of a static substrate in the desired crystallographic orientation.[58] Thus in these simulations periodic boundary conditions are imposed only in directions parallel to the surface plane. Because of the short range of the repulsive pair interactions and the finite-range of the atomic charge densities, it is sufficient to represent the static substrate by five solid layers. The lattice constant of the static substrate, and thus the dimensions of the calculational cell in the directions parallel to the surface plane are appropriate for the temperature of the study. From constant pressure simulations ($P_{\rm ext}=0$) of the bulk solid,[59] i.e., three-dimensional periodic boundary conditions, we have determined the coefficient of thermal expansion $\alpha=1.2\times10^{-5}$ K^{-1}, which compares with the experimental[57] value (at $T=300$ K) of 1.3×10^{-5} K^{-1}. The lattice constant at temperature T is given by $a(T)=a(T=0)\exp(\alpha T)$, where $a(T=0)=3.52$ Å and T is in degrees Kelvin.

In order to study the properties of the system at various temperatures we equilibrate the system at the desired temperature for $N_{\rm eq}$ integration time steps, $\Delta t=1.03\times10^{-15}$ sec, followed by a period of $N_d\Delta t$ over which data is accumulated and averaged. Since it is of particular importance in these studies to assure proper equilibration of the system at each temperature, we have used the following criteria that equilibrium at each of the selected temperatures was achieved: (a) absence of secular trend, versus time, in the kinetic energy and in the contributions to the potential energy, (b) a uniform profile of the kinetic temperature across the system, (c) absence of variations in the layer diffusion coefficients calculated for different segments of time, and (d) absence of periodic oscillations of interlayer spacing and registry in the crystalline part of the system and absence of variations (beyond statistical fluctuations) in characteristic properties (such as structure factors, and average number of atoms in layers). We found that to satisfy these criteria the following simulation procedure yields satisfactory results: (i) for $T\leq1000$ K, $N_{\rm eq}=10^3$; for $T=1250$ K, $N_{\rm eq}=5\times10^3$; for $T\geq1450$ K, $N_{\rm eq}=2\times10^4$ K, and (ii) $N_d=15\times10^3$ for $T\leq1712.5$ K and $N_d=25\times10^3$ for $T>1712.5$ K. Our simulations start from the low-temperature solid, and the system at each successively higher temperature is obtained starting from the equilibrated system at the temperature below it and adjusting the lattice constant to the new temperature. The canonical equilibrium ensembles at the desired temperatures are obtained via stochastic thermalization of particle velocities in conjunction with the velocity form of the Verlet integration algorithm.[60]

Integration of the equations of motion yields the phase-space trajectories for the system from which physi-

cal properties and their time evolution can be obtained. To facilitate the presentation of our results, we define for any property g_i, which depends on the phase-space point $(\mathbf{r}_i, \mathbf{v}_i)$ of atom i located at z_i (with $z=0$ set at the bottom of the dynamic slab and increasing toward the surface) a local density (per unit length) of that property at z by

$$\hat{\rho}_g(z)=\frac{1}{\sqrt{2\pi}\sigma}\sum_i g_i \exp[-(z-z_i)^2/2\sigma^2] . \quad (2a)$$

In our calculations a value of 0.125 Å (i.e., about 10% of the layer spacing $d=a/2\sqrt{2}$) is used for the width parameter σ. This allows us to exhibit our results as continuous profiles in the z direction.

The particle number density (per length) profiles, $\rho(z)$, are obtained by letting $g_i=1$ in Eq. (2a). Other properties are presented as per particle local densities

$$g(z)=\hat{\rho}_g(z)/\rho(z) . \quad (2b)$$

III. RESULTS

To investigate the variation of the properties of the system with temperature we show first in Figs. 1 and 2 the density and total energy profiles of the system versus distance (z) normal to the surface plane, for various temperatures. From Fig. 1 (see also last column in Table I) we note (see in particular the lower temperatures) that the surface region is relaxed,[61] (i.e., $\Delta_{12}<0$, where $\Delta_{12}=(d_{12}-d_{\text{bulk}})/d_{\text{bulk}}$); d_{12} is the distance in the z direction between layers 1 and 2 of the crystal and $d_{\text{bulk}}=a/2\sqrt{2}$. We remark that at finite temperatures we find that deeper layers exhibit only a very small degree of relaxation. In addition we observe a gradual change of the density profile with increase in temperature and the development of an "adlayer" (layer $l=0$) starting at $T\approx 1450$ K, which is absent at low temperatures. The atoms in this layer originate from the underlying layers, as may be seen from Table I. In addition we note that the distinction between layers is blurred as the melting temperature is approached [see in particular Fig. 1(b)].

Similar characteristics are exhibited in the per-particle total energy profiles versus z, shown in Fig. 2, where at each temperature the minima correspond to the layers' positions. In addition we include for comparison the energy profile for the liquid-to-vapor interface (dashed line) obtained from our previous simulations[53] of the equilibrium liquid-to-crystal and liquid-to-vapor interfaces at coexistence. We observe that for all temperatures the energy of particles in the top region of the solid (layers 1 and 2) is higher than in deeper layers because of the absence of particles on the vacuum side of the half-infinite system. In addition we remark that at $T=1733$ K the energy of particles in deep layers is close to that found in separate calculations for the bulk solid (-3.995 eV) and that of particles in the liquid region is close to the value for the melt (-3.775 eV) at the solid-to-melt coexistence point. Thus, the data shown in Fig. 2 indicates gradual formation of a liquid (or quasiliquid) film on top of the crystalline substrate. In particular we note that the energies of particles in the adlayer region are higher than in deeper regions, and that at the higher temperatures ($T>1700$ K) one may distinguish a liquid film region whose properties approach those of the bulk liquid. The interface between that liquid film and the underlying solid exhibits properties that are intermediate between

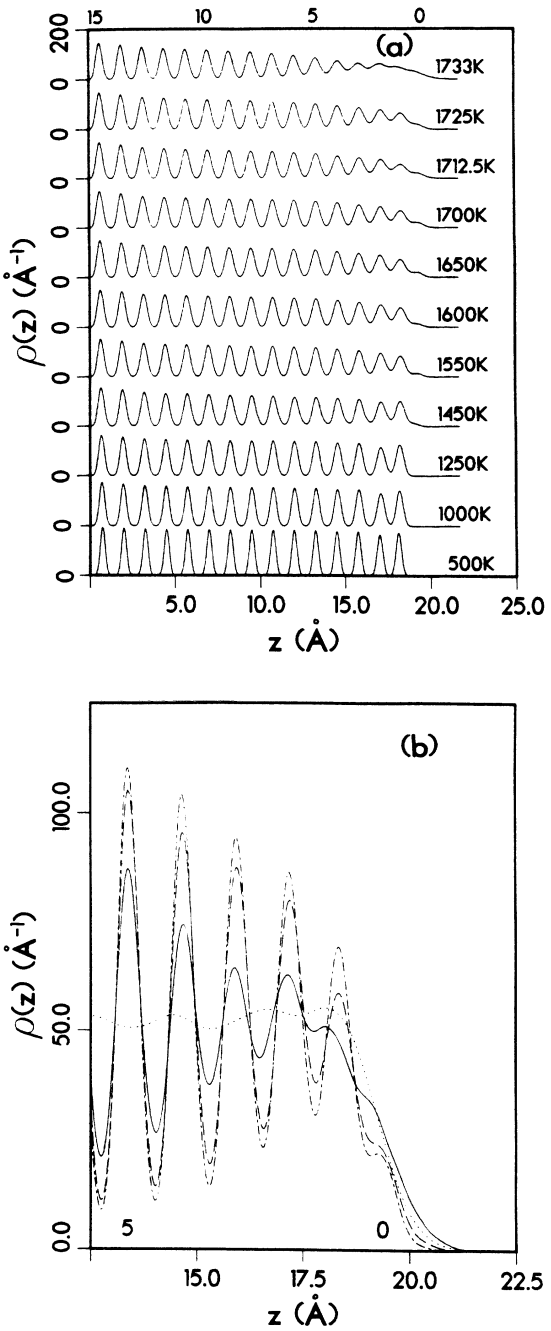

FIG. 1. (a) Equilibrium density profiles of the Ni(110) system vs distance z, normal to the surface plane for several temperatures. The layer's numbers are denoted on the top abscissa. Distance in Å, density in Å^{-1}. (b) Enlarged view of the density profiles in the surface region for $T\geq 1700$ K; dashed-dotted (1700 K), dashed (1712.5 K), solid (1733 K). In addition the density profile near the surface of liquid Nickel (Ref. 53) at the triplet point (1733 K) is shown, denoted by the dotted curve.

TABLE I. Equilibrium averaged number of particles in the topmost layers of Ni(110) at various temperatures. The first surface layer of the crystal is $l=1$. Layer $l=0$ corresponds to the adatom layer that starts to form at 1450 K. In the last column the percent of change in the spacing between layers 1 and 2, with reference to the bulk value, is given. The corresponding interlayer spacing relaxation at 0 K are $\Delta_{12}=-11.3\%$, $\Delta_{23}=1.5\%$, $\Delta_{34}=-0.8\%$, and $\Delta_{45}=0.3\%$.

	Layer Number						
T (K)	0	1	2	3	4	5	Δ_{12} (%)
500	0.0±0.0	70.0±0.0	70.0±0.0	70.0±0.0	70.0±0.0	70.0±0.0	−12
1000	0.0±0.0	70.0±0.0	70.0±0.0	70.0±0.0	70.0±0.0	70.0±0.0	−12
1250	0.0±0.0	70.0±0.0	70.0±0.0	70.0±0.0	70.0±0.0	70.0±0.0	−11
1450	3.9±1.0	66.1±1.0	70.0±0.0	70.0±0.0	70.0±0.0	70.0±0.0	−10
1550	8.1±1.7	63.4±2.6	69.3±2.0	69.4±1.3	69.9±0.8	70.0±0.6	−10
1600	10.1±2.5	61.0±3.2	70.0±2.1	69.4±1.6	69.6±1.0	70.0±0.7	−10
1650	12.9±2.3	59.6±2.9	69.3±2.4	68.7±1.8	69.7±1.2	70.0±0.9	−8
1700	14.6±2.4	59.3±3.1	68.4±2.7	68.6±2.0	69.6±1.2	69.7±1.0	−8
1712	18.1±2.9	56.7±4.5	68.3±3.1	68.7±2.2	68.9±1.7	69.6±1.2	−8
1725	15.8±2.9	58.9±3.8	67.6±2.7	69.1±2.2	69.3±1.6	69.5±1.3	−8
1733	26.4±4.0	58.1±5.3	70.2±3.8	62.1±3.7	66.5±3.4	68.7±2.6	

those of the liquid and solid, as expected.[53] Finally we note that throughout the process deeper layers in the system (e.g., $l \geq 8$) exhibit properties characteristic to the uniform bulk solid, and thus we use the properties of layers $8 \leq l \leq 10$ as reference bulk in analyzing the variations of the surface properties with increasing temperature (the influence of the static substrate may be seen for the 3–4 layers closest to it). Further evidence that for all $T<1733$ K a region exhibiting bulk properties is maintained is provided by the structure factors to be discussed later and by the values of the spacings between layers (for $7 \leq l \leq 11$) that are in agreement (to within 0.15%) with the bulk values at the corresponding temperatures.

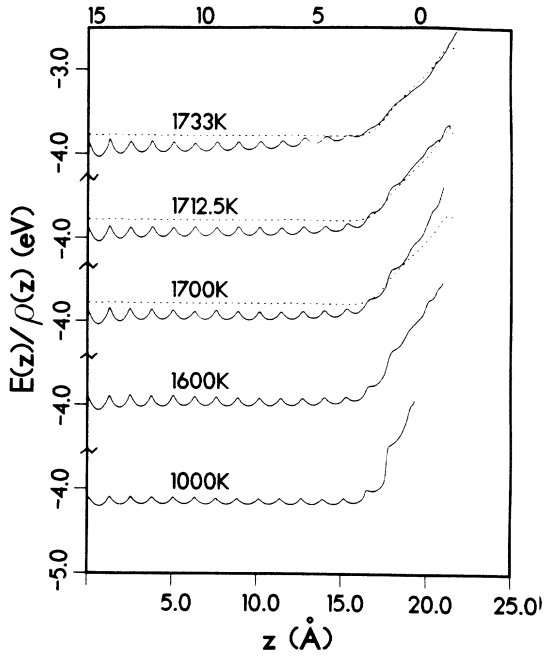

FIG. 2. Equilibrium total-energy per-particle profiles of the Ni(110) system, vs distance z normal to the surface plane for several temperatures. The minima correspond to layer positions. The layer's numbers are denoted on the top abscissa. Energy is in eV, and distance in Å. The dotted curve corresponds to the energy profile of the surface of liquid Ni at the triplet point (Ref. 53).

The structure of the system, and in particular the formation of the quasiliquid region can be analyzed using the layer pair-distribution functions, $p_l(r_\parallel)$, shown in Figs. 3(a)–3(f) for 1000 K $\leq T \leq$ 1733 K. The equilibrium $p_l(r_\parallel)$ functions are calculated as

$$p_l(r_\parallel)=\left\langle \frac{1}{n_l} \sum_{\substack{i,j\in l \\ (i\neq j)}} \frac{1}{2\pi r_\parallel} \delta(r_{ij,\parallel}-r_\parallel) \right\rangle , \tag{3}$$

where $r_{ij,\parallel}$ is the component of $\mathbf{r}_i-\mathbf{r}_j$ parallel to the surface plane, n_l is the instantaneous number of particles in layer l, the sums extend over the particles in layer l, and the angular brackets denote averaging over time. For reference, the pair-distribution function for the bulk liquid at the melting point[53] ($T=1733$) is shown (dashed line) for $T \geq 1700$ K. As seen from Figs. 3(a)–3(f), the intralayer structure in the topmost layers of the system ($l \lesssim 3$) changes gradually from crystalline to liquidlike character as the temperature increases. In this context we recall[53] that the crystal-to-melt interfaces of metals, as well as other materials, are characterized by a "liquid-layered" transition region (or quasiliquid region), extending typically over several layers, wherein structural and transport properties of the material are influenced by the crystalline field of the underlying substrate, exhibiting a gradual transition from solid-to-liquid properties. We note that for the adlayer ($l=0$) at $T<1733$ K, the probability of finding particles with separations beyond the first-neighbor shell is small, indicating a tendency for clustering, which persists even for $T \simeq 1733$ K [compare the ratio between peak heights in $p_l(r_\parallel)$ for $l=0$ and in the bulk].

The melting transition of the top region of the solid is further shown by the layer diffusion coefficients, shown in Fig. 4 versus temperature, calculated from the particle trajectories generated in these simulation according to

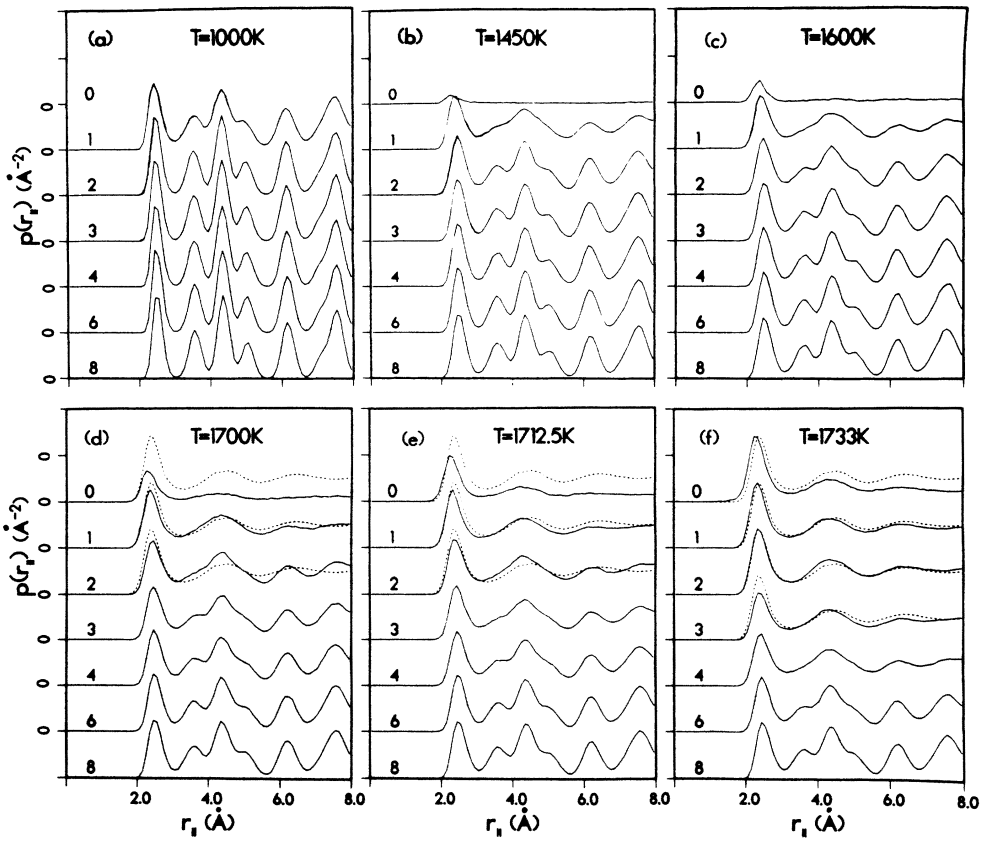

FIG. 3. Pair distribution functions $p_l(r_\parallel)$, in layers for the Ni(110) system equilibrated at several temperatures: (a) 1000 K; (b) 1450 K; (c) 1600 K; (d) 1700 K; (e) 1712.5 K; (f) 1733 K. Layer $l=0$ corresponds to the adlayer that forms at $T \gtrsim 1450$ K. Note the gradual transition from solid-to-liquid character upon increasing temperature. The dotted line in *d* through *f* corresponds to the bulk liquid at the melting point. The numbers by the curves indicate the layer's indices. Distance in unit of Å.

$$D_l = \lim_{t\to\infty} \frac{R_l^2(t)}{2n_d t} , \tag{4a}$$

where

$$R_l^2(t) = \left\langle \frac{1}{n_l} \sum_{i\in l} [\mathbf{R}_i(t+\tau) - \mathbf{R}_i(\tau)]^2 \right\rangle . \tag{4b}$$

In the preceding equations the sum includes all atoms in layer l at time τ, n_d is the dimensionality, and the angular brackets denote averaging over time origins, τ. The total diffusion coefficients ($n_d=3$) in the topmost layers of the system are shown in Fig. 4(a) and a decomposition ($n_d=1$) into diffusion coefficients along the atomic rows (in the $[1\bar{1}0]$ direction) and across the rows (in the [001] direction) are shown in Figs. 4(b) and 4(c), respectively. As is evident from these results, the layer diffusion coefficients are larger for regions closer to the vacuum interface (i.e., $D_l > D_{l+1}$) exhibiting a slow gradual increase until $T \gtrsim 1700$, and a marked enhancement in the diffusion rates for $T > 1700$ (note that the onset of the increase of D_l for the fourth layer occurs at a somewhat more elevated temperature than that corresponding to layers $l \leq 3$). These observations correlate with the structural variations at the surface region exhibited in Fig. 3. Finally, we remark that the coefficients for diffusion along the rows ($[1\bar{1}0]$ in Fig. 4(b)) are in general slightly higher than those for the direction across the rows ([001] in Fig. 4(c)), which may indicate a small enhanced tendency for disordering and eventual initiation of melting in the former direction. These observations correlate with anisotropic diffusion on the (110) surface of Pb close to the bulk melting, measured via quasielastic scattering of low-energy He atoms.[28(b)]

The observations discussed earlier are reflected and corroborated by the structure factors

$$S_l(\mathbf{g}_\alpha) = \frac{1}{n_l} \sum_{i\in l} e^{i\mathbf{g}_\alpha\cdot\mathbf{r}_i}, \quad \alpha = 1,2,3 , \tag{5}$$

calculated for the three reciprocal lattice vectors: $\mathbf{g}_1 = (2\pi/a)(2,\bar{2},0)$ along the atomic rows, $\mathbf{g}_2 = (2\pi/a)(0,0,2)$ across the rows, and $\mathbf{g}_3 = (2\pi/a)(2,2,0)$. As before, n_l is the instantaneous number of particles in layer l, the sum extends over the particles in layer l.

The equilibrium averaged (indicated in the following by angular brackets) squared magnitude of the layer structure factors corresponding to the three reciprocal lattice vectors for the Ni(110) system equilibrated at selected temperatures are shown in Fig. 5. We note first

that at low temperature [1000 K shown in Fig. 5(a)], the structure factors are constant throughout most of the system, exhibiting a decrease at the surface region. The deviation of $\langle |S_l(\mathbf{g}_\alpha)|^2 \rangle$ from unity originates from thermal vibrations and the decrease near the surface reflects the enhanced vibrational amplitudes of surface atoms. Note in particular the nonmonotonic behavior of $\langle |S_l(\mathbf{g}_3)|^2 \rangle$ near the surface [i.e., $\langle |S_1(\mathbf{g}_3)|^2 \rangle < \langle |S_2(\mathbf{g}_3)|^2 \rangle$] for

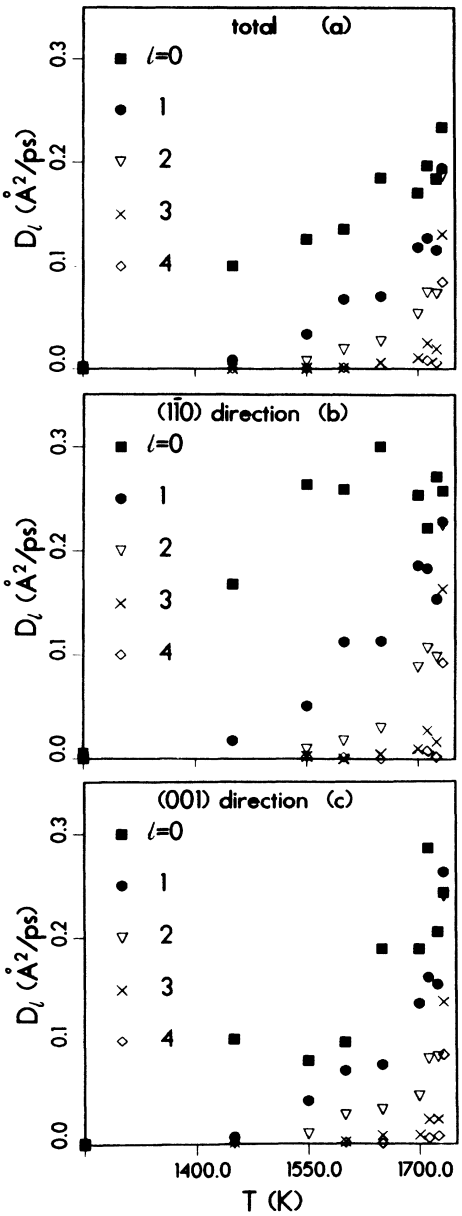

FIG. 4. Coefficients of diffusion in layers vs temperature, for the Ni(110) system. Solid squares correspond to the adlayer $l=0$; solid circles correspond to the first layer; inverted triangles $l=2$; X's denote the diffusion coefficients in layer 3 and diamonds correspond to those in the fourth layer. (a) Total diffusion coefficients; (b) and (c) diffusion coefficients along the atomic rows ([1$\bar{1}$0] direction) and across the rows ([001] direction), respectively. Note the marked increase in the rate of diffusion at $T \gtrsim 1700$ K (particularly for $l \leq 3$). Diffusion coefficients in units of (Å^2/ps) and temperature in degrees Kelvin.

$T < 1550$ K, which reflects a smaller root-mean-square (rms) vibrational amplitude in the direction normal to the surface (110) of the first-layer atoms than those of the second-layer atoms. Upon increasing the temperature, the magnitude of the surface factors decrease both in the bulk (because of enhanced vibrations) and in particular at the surface region (because of enhanced vibrations, generation of defects, and disorder). In Figs. 5(b)–5(f) we observe that the structure factors for $\mathbf{g}_2$ (circles) and $\mathbf{g}_3$ (triangles) corresponding to the first layer are lower than those for the adlayer (layer $l=0$), indicating a higher degree of order in the latter. Apparently the adlayer atoms, which for these temperatures originate mostly as a result of the generation of vacancies in the first crystalline atomic layer (see Table I), distort the structure of the underlying layer. This observation is corroborated by analysis of atomic configurations of the system and is similar to that observed previously[46(b)] in simulations of the onset of disorder in the Al(110) surface below the melting point.

The structural data, presented as the natural logarithm of the squared magnitude of the layer structure factors corresponding to layers $0 \leq l \leq 6$ plotted versus temperature is shown in Fig. 6. The behavior of the structure factors versus temperature exhibits two regimes: (i) a low-temperature regime, $T \lesssim 1450$ K, characterized for all layers by a slow monotonic decrease of $\langle |S_l(\mathbf{g}_\alpha)|^2 \rangle$ upon increasing the temperature and (ii) a high-temperature regime, $T \gtrsim 1450$ K, where the decrease of $\langle |S_l(\mathbf{g}_\alpha)|^2 \rangle$ with increase in temperature is more rapid for layers in the surface region of the material. In the harmonic approximation of solids (the Debye-Waller theory) $\ln\langle |S(\mathbf{g})|^2 \rangle$ is proportional to T. For crystals, deviations from linear dependence on temperature can be explained in terms of anharmonic vibrational effects. Considerations of these effects yield expressions[62–64] for $\ln\langle |S(\mathbf{g})|^2 \rangle$ that contain, in addition to the term linear in T, terms proportional to T^2 and T^3 and that can be used to fit the data. The coefficients of the quadratic and cubic terms depend on derivatives of the potential beyond the harmonic approximation and can be expressed within certain models in terms of characteristic material parameters, such as the Grüneisen and volume expansion coefficients.[64] Indeed the calculated data given in Figs. 6(a)–6(c) in the low-temperature regime can be fit by such expressions.[65] For the surface region, the behavior of the structure factors in the high-temperature regime cannot be fit using the above-mentioned expressions, reflecting the onset of defects and disorder [note also the first appearance of vacancies and adatoms ($l=0$), at 1450 K, shown in the data given in Table I].

We should note that an approximation common to most theories of the temperature dependence of the structure factors is the neglect of correlations between the displacements of different atoms as well as between the displacements of individual atoms in different directions. Obviously the accuracy and interpretation of the fit between the theoretical expressions and measured or calculated data depend upon the validity of these approximations. To examine this issue we have calculated correlations between atomic displacements from the particle tra-

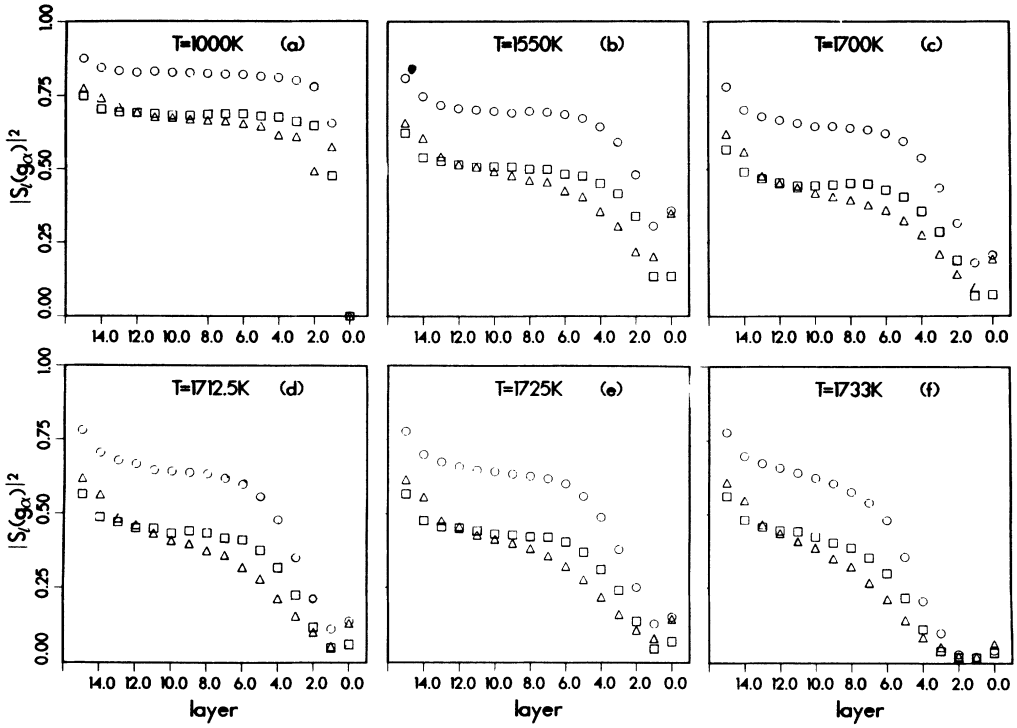

FIG. 5. Equilibrium averaged layer-structure factors squared $|S_l(\mathbf{g}_\alpha)|^2$, for $\alpha=1,2,3$, denoted by squares, circles, and triangles, respectively, vs layer number, at several temperatures: (a) 1000 K; (b) 1550 K; (c) 1700 K; (d) 1712.5 K; (e) 1725 K; (f) 1733 K. Note the lower magnitudes of the structure factors at the surface region, and their decrease upon increasing temperature, with the onset of surface melting for $T \gtrsim 1700$ K. The higher values of $|S_0(\mathbf{g}_2)|^2$ and $|S_0(\mathbf{g}_3)|^2$ than those corresponding to the first layer ($l=1$) seen in (b) through (f) indicate a higher degree of order in the adlayer than in the first solid layer, which distorts due to the creation of vacancies and the subsequent formation of the adlayer.

jectories generated by the simulations. We find that while the displacements of individual atoms in different directions are essentially uncorrelated, the correlations between the displacements of nearest-neighbor (NN) atoms are significant (as large as $\sim 50\%$ of the mean-square atomic displacements), and are of larger magnitude for atoms both of which are in the same atomic row (i.e., $[1\bar{1}0]$ direction) than those for atoms which are NN to one another in the direction across the atomic rows ([001] direction). In addition the correlations are largest for displacements along the $[1\bar{1}0]$ direction and are smallest for displacements along the [110] direction (perpendicular vibrations). Furthermore, larger correlations are found for atoms in the surface region of the material (3–5 topmost layers). Thus on the (110) surface the vibrational correlations, like the vibrational amplitudes (see later) and atomic transport properties, exhibit a crystallographical anisotropy with an enhancement along the $[1\bar{1}0]$ direction. These results indicate that the values of quantities (such as rms vibrational amplitudes and anharmonicity coefficients) extracted from fits to data using the above-mentioned theoretical expressions may be affected by the neglect of correlations in the theory. Since the focus of this paper is on disordering and premelting phenomena, we defer a detailed analysis of the anharmonic effects and correlations to a future publication.[65]

The data given in Fig. 6 provides further evidence for the anisotropy of properties at the (110) surface.[20,22,28(b),46(b)] Comparing the data in Figs. 6(a)–6(c) corresponding to the surface region, we observe that the one for $\mathbf{g}_1$ [Fig. 6(a)] is the lowest (more negative) in both temperature regimes. This indicates a larger rms vibrational amplitude parallel to the surface plane along the atomic rows ($[1\bar{1}0]$ direction). This conclusion correlates with our previous observations concerning enhanced diffusion and tendency to disorder in the $[1\bar{1}0]$ direction (see discussion following Fig. 4).

A direct measure of the mean vibrational amplitudes can be obtained from the particle trajectories generated in the simulation. Mean-squared amplitudes averaged over layers at 1250 K (below the onset of disorder) are shown in Fig. 7, for three orthogonal directions. As is evident, the vibrational amplitudes in the surface region are higher than in the bulk. We also note that the magnitude of the vibrational amplitude of second-layer atoms in the normal direction is the highest, and is larger than the amplitude of vibration in that direction for the topmost layer ($l=1$) of the solid (see also our comments in the context of our discussion of the structure factors). The enhancement of the vibrational amplitudes of second-layer atoms perpendicular to the surface plane is in contrast to the monotonic decrease away from the surface found in simulations employing pairwise (Lennard-Jones) potentials[66] and may be unique to metals reflecting

the many-body nature of cohesion in these materials.

We turn next to a discussion of the mechanisms and energetics underlying the disordering leading to the nucleation, at the surface, of melting (in fact gradual surface premelting) of the material. As shown in Table I and as noted in our discussion of the structure factors, the onset of disorder involves the generation of vacancies in the topmost layer ($l=1$) of the crystal at ~ 1450 K and the associated development of the adlayer ($l=0$). We also note that at higher temperature vacancies in deeper layers begin to appear. In this context we should emphasize the dynamic nature of the process as observed via analysis of particle trajectories revealing a host of intralayer and interlayer vacancy migration mechanisms. In Fig. 8 we plot the logarithm of the average number of adatoms ($l=0$) and vacancies in the first layer versus $(k_B T)^{-1}$. The fact that the slopes of the adlayer and first-layer data are not parallel to each other reflects the fact that at $T > 1450$ K not all the atoms in the adlayer ($l=0$) originate from the first layer ($l=1$). Using the slope of the data for $l=1$ in Fig. 8 up to 1700 K (above

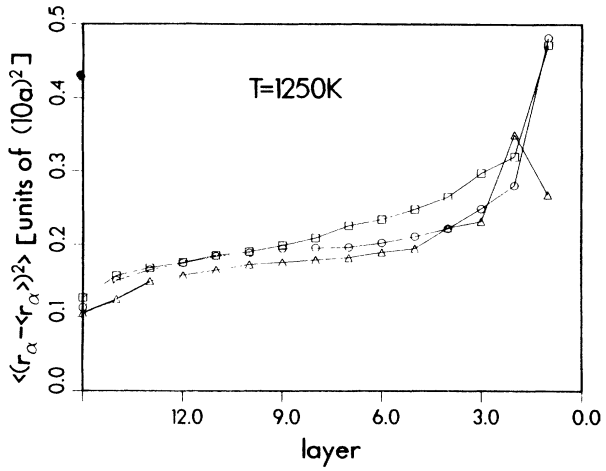

FIG. 7. Mean square displacements. [$\langle (r_\alpha - \langle r_\alpha \rangle)^2 \rangle$, α denotes displacement direction] of atoms averaged over layers, below the onset of surface disorder, $T=1250$ K. The symbols correspond to displacement along the atomic rows ([1$\bar{1}$0] direction, squares); across the rows ([001] direction, circles); and normal to the surface ([110] direction, triangles). The mean square displacements are given in units of $(10a)^2$, where a is the lattice constant, $a=3.573$ Å at 1250 K.

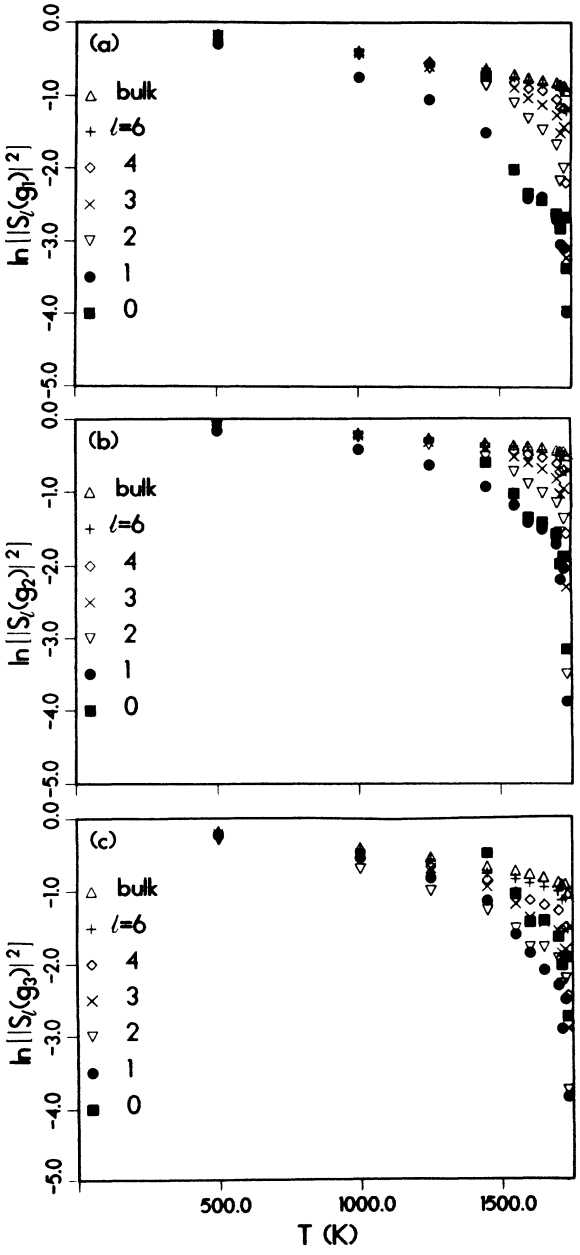

FIG. 6. Natural logarithm of the squared magnitude of the equilibrium averaged layer-structure factors, $|S_l(\mathbf{g}_\alpha)|^2$, for $\mathbf{g}_1$ [in (a)], $\mathbf{g}_2$ [in (b)], and $\mathbf{g}_3$ [in (c)] vs temperature. The symbols corresponding to the various layers are defined in the figure. Temperature in degrees Kelvin.

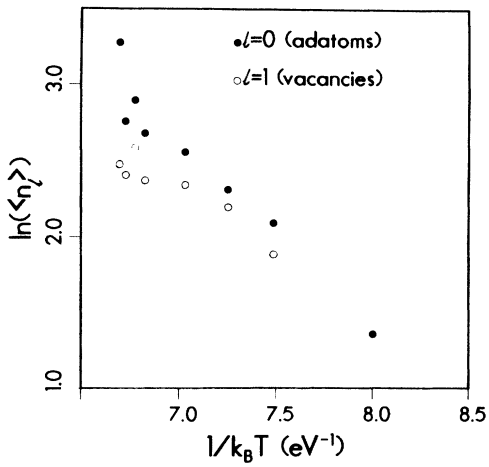

FIG. 8. Natural logarithm of the equilibrium average number of adatoms ($l=0$, closed circles) and vacancies in the first layer ($l=1$, open circles) vs $(k_B T)^{-1}$ in units of eV^{-1}. Note the linear relation for the lower temperatures $T \lesssim 1700$ K.

which premelting of the surface layer occurs) we estimate a vacancy-adatom-formation energy of ~ 1.0 eV.

The vacancy-formation energy, E_{vf}, can be defined as

$$E_{vf}=E(N-1,1)-E(N,0)-E_s \ , \tag{6}$$

where $E(N-1,1)$ is the energy of the solid containing $(N-1)$ atoms and a single vacancy, $E(N,0)$ is the energy of the perfect solid, and E_s (>0) is the sublimation energy (negative of the cohesive energy per atom in the perfect infinite crystal) of the system. Similarly the adatom-formation energy E_{af} can be defined as

$$E_{af}=\tilde{E}(N+1,1)-E(N,0)+E_s \ , \tag{7}$$

where $\tilde{E}(N+1,1)$ is the energy of the solid containing $(N+1)$ atoms, one of which is an adatom. It is difficult to obtain E_{vf} and E_{af} at a specified finite temperature from the simulations because the small energy differences are obscured by the fluctuations in the total energy. Using a conjugate-gradient energy minimization (i.e., relaxation) in conjunction with the EAM potentials, we have determined first the zero-temperature values for the following quantities: $E_s=4.447$ eV (compared to the experimental value[67] of 4.45 eV); $E_{af}=0.307$ eV, and $E_{vf}=1.386$ in the infinite bulk solid (compared to the experimental value[68] of 1.4 eV). In this context we remark that in fitting the EAM potential parameters[56] only the *bulk* sublimation and vacancy formation energies as well as bulk elastic constants have been used. Therefore, the values obtained for the energetics of the surface region of the material are consequences of the EAM potentials rather than fitted values. The cohesive energy of atoms in different layers, $E(l)$, is given in Table II. E_l is given by the term in large square brackets in Eq. (1) calculated for atom i in layer l. We note that this decomposition of E_{coh} is within the context of the parametrization of the EAM potentials[56] used by us, and in general is nonunique. Obviously, $E(l)$ is of smaller magnitude (less negative) for atoms in the surface layers, converging to $-E_s$ in deeper layers of the semi-infinite solid. The surface energy of Ni(110), E_{surf} can be obtained from the $E(l)$ values given in Table II as[52(a)]

$$E_{surf}=\sum_l [E(l)-(-E_s)] \ , \tag{8}$$

yielding $E_{surf}=0.9312$ eV/atom (i.e., 1700 erg/cm^2) compared to the measured[69] crystal-vapor surface energy (1725 erg/cm^2), which represents an average over several crystal faces, and to the value obtained by using a different parametrization of the EAM potentials[52(a)] (1740 erg/cm^2).

From Table II the single vacancy-formation energy [with and without relaxation, $E_{vf}(l)$ and $E^0_{vf}(l)$, respectively] is smallest in the topmost layer ($l=1$) and is largest in the second layer. The magnitude of the lattice relaxation energy contribution, $E_{v,\text{relax}}(l)$ to $E_{vf}(l)$, is largest for $l=1$ and in general is of small relative magnitude (the value in the bulk, -0.011 eV, is in agreement with that obtained in previous calculations[52(a)]). The fact that $E_{vf}(l)$ in the second layer ($l=2$) of the solid is largest can be explained by examining the effect of a second-layer vacancy on the cohesive energy of neighboring first-layer atoms. To analyze the energetics of vacancy formation in the topmost layers of the solid, in Table III we give the number $[N_{NN}(l,l')]$ of nearest neighbors in layer l' to a vacancy in layer l and the change in the cohesive energy of an atom in layer l', which is a NN to the vacancy in layer l $[\Delta E_{NN}(l,l')]$. In addition we calculate the difference between the formation energy of a vacancy in the lth layer $[E_{vf}(l)$, see Table II] and the nearest-neighbors contribution to $E_{vf}(l)$,

$$\Delta_l=[E_{vf}(l)+E_s]-\left[\sum_{l'} N_{NN}(l,l')\Delta E_{NN}(l,l')-E(l)\right] \ , \tag{9}$$

where $E(l)$ [i.e., the cohesive energy of an atom in layer l of the perfect solid] is given in Table II. We note that $\Delta E_{NN}(l,1)$ is the largest, regardless of l (i.e., for a vacancy in the first, second, or third layer). In addition, the number of first-layer nearest-neighbors is largest (i.e., 4) for a second-layer vacancy, which results in a larger second-layer vacancy formation energy. Finally, to justify the aforementioned discussion, which is based on nearest-neighbor interactions, we note (see bottom row of Table III) that the relative contributions of neighbors beyond the first NN are small (less than 3%) in all cases.

The formation energy of a vacancy-adatom pair, with the two separated by a large distance, can be calculated

TABLE II. Energies in layers ($l=1$ is the topmost layer of the solid) at $T=0$ K. $E(l)$ is the cohesive energy [see Eq. (1)] of atoms in layer l. $E^0_{vf}(l)$ is the vacancy formation energy without lattice relaxation [see Eq. (6)]. $E_{v,\text{relax}}(l)$ is the relaxation energy following the vacancy formation. $E_{vf}(l)=E^0_{vf}(l)+E_{v,\text{relax}}(l)$ is the vacancy formation energy including lattice relaxation. $E_{vf}(l)+E^{\infty}_{af}$ [see Eqs. (6) and (7)] is the formation energy (including relaxation) of a vacancy adatom pair, with the adatom far from the vacancy. Energies are given in electron volts.

l	$E(l)$	$E^0_{vf}(l)$	$E_{v,\text{relax}}(l)$	$E_{vf}(l)$	$E_{vf}(l)+E^{\infty}_{af}$
1	−3.6937	0.366	−0.087	0.279	0.586
2	−4.2843	1.731	−0.076	1.655	1.962
3	−4.4305	1.604	−0.077	1.526	1.833
4	−4.4481	1.403	−0.012	1.391	1.698
5	−4.4472	1.395	−0.012	1.384	1.691
6	−4.4470	1.397	−0.011	1.385	1.692
8	−4.4470	1.397	−0.011	1.385	1.693
10	−4.4470	1.397	−0.011	1.385	1.693

TABLE III. Energetics of vacancy formation in different layers $1 \le l \le 3$. $N_{NN}(l,l')$ is the number of nearest neighbors (NN) to the vacancy in layers $1 \le l' \le 5$. $\Delta E_{NN}(l,l')$ is the change in the cohesive energy of a nearest-neighbor atom to the vacancy, in the specified layer l'. Δ_l is the contribution to $E_{vf}(l)$ from more distant neighbors, see Eq. (9).

	Vacancy in $l=1$		Vacancy in $l=2$		Vacancy in $l=3$	
l'	$N_{NN}(l,l')$	$\Delta E_{NN}(l,l')$	$N_{NN}(l,l')$	$\Delta E_{NN}(l,l')$	$N_{NN}(l,l')$	$\Delta E_{NN}(l,l')$
1	2	0.1887	4	0.2068	1	0.1618
2	4	0.1117	2	0.1223	4	0.1268
3	1	0.0947	4	0.1173	2	0.1016
4	0		1	0.1057	4	0.1064
5	0		0		1	0.1060
Δ_l		0.1134		0.1710		0.1390
$\frac{\Delta_l}{E_{vf}(l)+E_s}$		0.024		0.028		0.023

from Eqs. (6) and (7). The values thus obtained are given under $E_{vf}(l)+E_{af}^{\infty}$ in Table II. It is interesting to compare the value for the topmost layer (0.586 eV) with that obtained when the adatom is located in a site on the surface adjacent to the vacancy. When the adatom and vacancy are nearest neighbors to each other the value obtained for the formation energy of the pair is 1.086 eV, which is larger than that obtained for infinite separation. The convergence to the infinite separation value is very rapid (i.e., positioning the adatom at the next further site from the vacancy yields 0.558 eV). These results show that the vacancy-adatom interaction is repulsive and of short range.

Having discussed in some detail the energetics of formation of single vacancies and vacancy-adatom pairs we consider next the formation of divancies. As seen from Table IV the formation energy of a divacancy in layers l and l' $[E_{2vf}(l,l')]$ is less than the sum of the corresponding single-vacancy formation energies (most pronounced for divacancies in the first layer). The formation energy of two NN adatoms (far removed from any vacancies) equals 0.184 eV, and is also much smaller than $2E_{af}=0.614$. Using these results we find (see Table IV) that $E_{2vf}(l)+E_{2af}$, i.e., the formation energy of divacancy-diadatom pair is *lower* than that corresponding to the formation of a single vacancy-adatom pair (in other words two is better than one). In fact we have observed that in the simulations the initial defect that formed on the surface was a divacancy-diatom pair, i.e., a near simultaneous jump of two nearest-neighbor atoms from the topmost layer ($l=1$) to the adatom layer ($l=0$).

TABLE IV. Formation energies, $E_{2vf}(l,l')$, of nearest-neighbor divacancies in layers l and l', the sum of two single-vacancy formation energies $E_{vf}(l)+E_{vf}(l')$, in layers l and l' and $E_{2vf}(l,l')+2E_{2af}$, where $E_{2af}=0.184$ eV is the formation energy of two nearest-neighbor adatoms far removed from any vacancies. Energies are given in eV.

l	l'	$E_{2vf}(l,l')$	$E_{vf}(l)+E_{vf}(l')$	$E_{2vf}(l,l')+E_{2af}$
1	1	0.207	0.558	0.391
2	2	3.203	3.310	3.387
1	2	1.640	1.934	1.824
bulk		2.607	2.772	2.791

Further evolution of disorder involved generation of new vacancies adjacent to previously formed vacancies as well as divacancy formation. At the beginning of the process ($T \approx 1450$ K) the adatoms originate exclusively from the first layer. At higher temperatures, vacancies generate in deeper layers via promotion of atoms to vacancies in the layer above. Furthermore, the fact that $E_{2af} < 2E_{af}$ is reflected in the clustering tendency that we have observed of atoms in the adlayer (see our discussion in the context of the pair-distribution functions, Fig. 3).

The development of a large concentration of mobile vacancies (and adatoms) via the above-mentioned mechanisms, and the accompanying distortions of the lattice lead at ~ 1700 K to the loss of crystalline structural and dynamical character and the emergence of a quasiliquid region, as reflected in our analysis of the pair distributions, structure factors, and transport properties.

IV. SUMMARY

In this study we investigated the behavior of the (110) surface of nickel over a wide temperature range using molecular-dynamics simulations and employing the many-body potentials obtained via the embedded-atom method. In this context we should remark that in studies of surface premelting employing Lennard-Jones potentials,[47–51] the disordering of the surface region starts at a lower temperature (relative to the bulk melting point) than is typically observed and calculated for metals and has been associated with a roughening transition. However, as is well known, these pairwise interactions fail to provide a proper description of metallic systems, casting doubt on the applicability of these studies for the analysis of the energetics and dynamics of premelting processes in metals.

Our results show that structural and dynamical (transport) properties of the system may be discussed in terms of two temperature regimes: (i) At low temperatures ($T \lesssim 1450$ K) the response of the system to increase in temperature can be explained in terms of anharmonic vibrational effects, and for these temperatures there is no indication for loss of long-range order due to defect formation and/or significant atomic diffusion. Atoms in the surface region of the material vibrate with larger mean-square vibrational amplitudes than those in deeper layers

in the material, and their displacements are largest in the [1$\bar{1}$0] direction (along the atomic rows) reflecting the crystallographic anisotropy of the surface. Furthermore analysis[65] of the temperature behavior of the surface factors versus temperature indicates that the anharmonicity of the vibrations in the [001] direction (across the atomic rows) is larger than that along the [1$\bar{1}$0] and the [110] directions. (ii) The onset of disorder occurs at $T \approx 1450$ K via the generation of vacancies in the topmost layer of the solid accompanied by the formation of an adlayer, a sharp drop in the structure factors, and an increase in diffusion at the surface. We observed that the mechanism underlying this process involves initially the formation of divacancy-diadatom pairs. Further development of disorder and its propagation upon increasing the temperature to the second and third layers of the solid occur via generation of vacancies adjacent to previously formed ones (in the same layer or in the layers above), accompanied by the formation of an adlayer, destabilization of the lattice structure, gradual loss of long-range order and higher diffusion rates (of atoms and vacancies). The process culminates at $T \sim 1700$ K in the formation of a quasiliquid surface region (extending over the adlayer and 2–3 layers of the original solid) characterized by interfacial liquidlike structural and atomic transport properties. In this context it is of interest to note that the approach to the quasiliquid state is characterized by a crystallographic anisotropy (enhanced loss of long-range order and larger diffusion rates along the [1$\bar{1}$0] direction) and that at all temperatures prior to the melting of the material (at ~ 1733 K) the adlayer exhibits a larger degree of order than the adjacent layer underneath it.

From these observations we conclude that disordering of the surface region occurs first via anharmonic effects ($T < 1450$ K), the generation of top layer vacancies accompanied by the formation of an adlayer at $T \simeq 1450$ K, the *gradual thickening* of the defective surface region (i.e., vacancy formation in deeper layers) at $T > 1450$ K, and the eventual formation of a quasiliquid surface region (premelting) at $T \simeq 1700$ K. Above 1700 K the rate of loss of long-range order in the crystal and the increase in diffusion evolve (both in magnitude and spatially) in a "catastrophic" manner.

It is of interest to remark that while the vacancy driven mechanism of disordering found in this study is similar to that found in a previous study[46] of the (110) surface of aluminum, the temperature at which the Ni(110) surface premelts (formation of the quasiliquid layer) found in the present study is much closer to the bulk melting temperature of the material, then that found for Al(110). This may be regarded as a reduced tendency of nickel to premelt. It is of interest to note that this finding is consistent with that reached by van der Veen *et al.*[1] on the basis of thermodynamic considerations. A systematic investigation of the microscopic energetic and dynamic origins underlying the propensity of materials to premelt is underway.

ACKNOWLEDGMENTS

This work was supported by the U.S. Department of Energy under Grant No. DE-FG05-86ER-45234. Useful comments and communications by E. Conrad of his results prior to publication are gratefully acknowledged.

[1]See review by J. van der Veen, B. Pluis, and A. W. Denier van der Gon, in *Chemistry and Physics of Solid Surfaces* (Springer-Verlag, Berlin, 1989), Vol. II.

[2]J. G. Dash, in *Proceedings of the Solvay Conference on Surface Science: Austin, Texas, 1987,* Vol. 14 of *Springer Series in Surface Science,* edited by F. W. de Wette (Springer-Verlag, New York, 1988), p. 142.

[3]M. Faraday, Proc. R. Soc. London **10**, 440 (1860); in *Faraday Diary* (Bell, London, 1933), Vol. II, pp. 79–81; see also W. A. Weyl, J. Colloid Sci. **6**, 389 (1951).

[4]G. Tammann, Z. Phys. Chem. **68**, 205 (1910); Z. Phys. **11**, 609 (1910).

[5]J. F. van der Veen and J. M. W. Frenken, Surf. Sci. **178**, 382 (1986), and references therein.

[6]D. Nenow, Prog. Cryst. Growth Charact. **9**, 1893 (1984), and references therein.

[7]J. W. M. Frenken and J. F. van der Veen, Phys. Rev. Lett. **54**, 134 (1985).

[8]J. W. M. Frenken, P. M. J. Maree, and J. F. van der Veen, Phys. Rev. B **34**, 7506 (1986).

[9]J. F. van der Veen, Surf. Sci. Rep. **5**, 199 (1985).

[10]Da-Ming Zhu and J. G. Dash, Phys. Rev. Lett. **57**, 2959 (1986).

[11]Da-Ming Zhu and J. G. Dash, Phys. Rev. Lett. **60**, 432 (1988).

[12]G. Fritsch, R. Lachner, H. Diletti, and E. Luscher, Philos. Mag. A **46**, 829 (1982).

[13]G. Fritsch, H. Diletti, and E. Luscher, Philos. Mag. A **50**, 545 (1984).

[14]R. H. Willens, A. Kornblit, L. R. Testardi, and S. Nakahara, Phys. Rev. B **25**, 290 (1982).

[15]J. L. Tallon, W. H. Robinson, and S. I. Smedley, J. Phys. Chem. **82**, 1277 (1978).

[16]D. Beaglehole and D. Nason, Surf. Sci. **96**, 357 (1980).

[17]Y. Furukawa, M. Yamato, and T. Kuroda, J. Cryst. Growth **82**, 665 (1987).

[18]E. G. McRae and R. A. Malic, Phys. Rev. Lett. **58**, 1437 (1987).

[19]P. von Blanckenhagen, W. Schommers, and V. Voegele, J. Vac. Sci. Technol. A **5**, 649 (1987).

[20]K. C. Prince, U. Breuer, and H. P. Bonzel, Phys. Rev. Lett. **60**, 1146 (1988).

[21]H.-N. Yang, T.-M. Lu, and G.-C. Wang (unpublished).

[22]For recent low-energy electron diffraction studies of the Ni(110) surface at various temperatures see E. Conrad (private communication, unpublished).

[23]G. Devaud and R. H. Willens, Phys. Rev. Lett. **57**, 2683 (1986).

[24]J. Krim, J. P. Coulomb, and J. Bouzidi, Phys. Rev. Lett. **58**, 583 (1987).

[25]A. Kouchi, Y. Furukawa, and T. Kuroda, J. Phys. (Paris) Colloq. **48**, Suppl. 3, C1-675 (1987).

[26]P. H. Fuoss, L. J. Norton, and S. Brennan, Phys. Rev. Lett.

60, 2046 (1988).
[27]N. Bienfait, Europhys. Lett. **4**, 79 (1978).
[28](a) J. W. M. Frenken, J. P. Toennies, and Ch. Woll, Phys. Rev. Lett. **60**, 1727 (1988); (b) J. W. M. Frenken, B. J. Hinch, J. P. Toennies, and Ch. Woll (unpublished); (c) J. W. M. Frenken, J. P. Toennies, Ch. Woll, B. Pluis, A. W. Denier van der Gon, and J. F. van der Veen, in *The Structure of Surfaces,* Vol. II of *Springer Series in Surface Sciences,* edited by J. F. van der Veen and M. A. Van Hove (Springer, Berlin, 1988).
[29]J. W. M. Frenken, J. Vac. Sci. Technol. **A7**, 2147 (1989).
[30]K. D. Stock and E. Menzel, Surf. Sci. **61**, 272 (1976).
[31]K. D. Stock, Surf. Sci. **91**, 655 (1980).
[32]W. K. Burton, N. Cabrera, and F. C. Frank, Philos. Trans. R. Soc. London **243**, 299 (1951).
[33]F. A. Lindemann, Z. Phys. **14**, 609 (1910).
[34]J. N. Stranski, Z. Phys. **119**, 22 (1942).
[35]J. Frenkel, *Kinetic Theory of Liquids* (Clarendon, London, 1946), pp. 425–6.
[36]J. K. Kristensen and R. M. J. Cotterill, Philos. Mag. **36**, 437 (1977).
[37]T. Kuroda and R. Lacmann, J. Cryst. Growth **56**, 189 (1982); D. Nenow and A. Trayanov, *ibid.* **79**, 801 (1986).
[38]L. Pietronero and E. Tosatti, Solid State Commun. **32**, 255 (1979).
[39]C. S. Jayanthi, E. Tosatti, A. Fasolino, and L. Pietronero, Surf. Sci. **152/153**, 155 (1985).
[40]C. S. Jayanthi, E. Tosatti, and L. Pietronero, Phys. Rev. B **31**, 3456 (1985).
[41]A. Trayanov and E. Tosatti, Phys. Rev. Lett. **59**, 2207 (1987); Phys. Rev. B **38**, 6961 (1988).
[42]G. An and M. Schick, Phys. Rev. B **39**, 9722 (1989).
[43]R. Lipowsky, Phys. Rev. Lett. **49**, 1575 (1982).
[44]R. Lipowsky and W. Speth, Phys. Rev. B **28**, 3983 (1983).
[45]R. Lipowsky, U. Breuer, K. C. Prince, and H. P. Bonzel, Phys. Rev. Lett. **62**, 913 (1989).
[46](a) P. Stoltze, J. K. Norskov, and U. Landman, Phys. Rev. Lett. **61**, 440 (1988); (b) Surf. Sci. (to be published).
[47]J. Q. Broughton and G. H. Gilmer, Acta Metall. **31**, 845 (1983).
[48]J. Q. Broughton and G. H. Gilmer, J. Chem. Phys. **79**, 5095 (1983); **79**, 5105 (1983); **79**, 5119 (1983).
[49]V. Pontikis and P. Sindzingre, Phys. Scr. T **19**, 375 (1987).
[50]V. Rosato, G. Cicotti, and V. Pontikis, Phys. Rev. B **33**, 1860 (1986).
[51]S. Valkealahti and R. M. Nieminen, Phys. Scr. **36**, 646 (1987).
[52](a) M. S. Daw and M. I. Baskes, Phys. Rev. B **29**, 6443 (1984); (b) S. M. Foiles, M. I. Baskes, and M. S. Daw, *ibid.* **33**, 7983 (1986).
[53]E. T. Chen, R. N. Barnett, and U. Landman, Phys. Rev. B **40**, 924 (1989).
[54]K. W. Jacobson, J. K. Norskov, and M. J. Puska, Phys. Rev. B **35**, 7423 (1987); J. K. Norskov, *ibid.* **26**, 2875 (1982).
[55]P. Hohenberg and W. Kohn, Phys. Rev. B **136**, 864 (1964).
[56]S. M. Foiles, Phys. Rev. B **32**, 3409 (1985).
[57]*Handbook of Chemistry and Physics,* edited by R. C. Weast (CRC, Cleveland, 1974).
[58]The two-dimensional unit cell in the surface plane is defined by the unit vectors $\mathbf{a}_1=(a/2)(1,-1,0)$ and $\mathbf{a}_2=a(0,0,1)$, which lie along and across the atomic rows, respectively. The third direction is defined by the vector $\mathbf{a}_3=(a/2)(1,0,1)$. The spacing between atomic layers is $d=a/2\sqrt{2}$, and a is the fcc cube edge length that for nickel is equal to 3.52 Å at 0 K and 3.593 Å at 1700 K. The dimensions of the calculational cell in the surface plane are 10 $\mathbf{a}_1$ and 7 $\mathbf{a}_2$, with 70 atoms/layer.
[59]M. Parinello and A. Rahman, J. Appl. Phys. **52**, 7182 (1981).
[60]J. R. Fox and H. C. Anderson, J. Phys. Chem. **88**, 4019 (1984).
[61]U. Landman, N. R. Hill, and M. Mostoller, Phys. Rev. B **21**, 448 (1980); R. N. Barnett, U. Landman, and C. L. Cleveland, *ibid.* **28**, 1685 (1983); R. N. Barnett, U. Landman, C. L. Cleveland, and R. H. Rast, J. Vac. Sci. Technol. **3**, 1574 (1985).
[62]A. A. Maradudin and P. A. Flinn, Phys. Rev. **129**, 2529 (1963).
[63]B. T. M. Willis, Acta Cryst. A **25**, 277 (1969).
[64]J. Prakash and M. P. Hemkar, J. Phys. Soc. Jpn. **36**, 1608 (1974).
[65]R. N. Barnett and U. Landman (unpublished).
[66]W. Schommers, *Structure and Dynamics of Surfaces I,* Vol. 41 of *Topics in Current Physics,* edited by W. Schommers and P. von Blanckenhagen (Springer, Berlin, 1986), p. 199, and references therein.
[67]*Metal Reference Book,* edited by C. J. Smith (Butterworth, London, 1976).
[68]*Vacancies and Interstitials in Metals,* edited by A. Seeger, D. Schumacher, W. Schilling, and J. Diehl (North-Holland, Amsterdam, 1970).
[69]M. C. Inman and H. R. Tippler, Metallogr. Rev. **8**, 105 (1963).